Cerebral Cortex, October 2021;31: 4628–4641

https://doi.org/10.1093/cercor/bhab110
Advance Access Publication Date: 17 May 2021
Original Article

ORIGINAL ARTICLE

Maximum Entropy Principle Underlies Wiring Length Distribution in Brain Networks

Yuru Song[1], Douglas Zhou[2,3,4] and Songting Li[2,3,4]

[1]Neuroscience Graduate Program, University of California, San Diego, CA, USA, [2]School of Mathematical Sciences, Shanghai Jiao Tong University, Shanghai 200240, China, [3]Institute of Natural Sciences, Shanghai Jiao Tong University, Shanghai 200240, China and [4]Ministry of Education Key Laboratory of Scientific and Engineering Computing, Shanghai Jiao Tong University, Shanghai 200240, China

Address correspondence to Douglas Zhou. Email: zdz@sjtu.edu.cn: Songting Li. Email: songting@sjtu.edu.cn

Abstract

A brain network comprises a substantial amount of short-range connections with an admixture of long-range connections. The portion of long-range connections in brain networks is observed to be quantitatively dissimilar across species. It is hypothesized that the length of connections is constrained by the spatial embedding of brain networks, yet fundamental principles that underlie the wiring length distribution remain unclear. By quantifying the structural diversity of a brain network using Shannon's entropy, here we show that the wiring length distribution across multiple species—including *Drosophila*, mouse, macaque, human, and *C. elegans*—follows the maximum entropy principle (MAP) under the constraints of limited wiring material and the spatial locations of brain areas or neurons. In addition, by considering stochastic axonal growth, we propose a network formation process capable of reproducing wiring length distributions of the 5 species, thereby implementing MAP in a biologically plausible manner. We further develop a generative model incorporating MAP, and show that, for the 5 species, the generated network exhibits high similarity to the real network. Our work indicates that the brain connectivity evolves to be structurally diversified by maximizing entropy to support efficient interareal communication, providing a potential organizational principle of brain networks.

Key words: brain structure, maximum entropy, structural diversity, wiring length

Introduction

The dynamics of a brain network is substantially affected by its comprehensive connectivity structure. For instance, it has been shown that the functional connectivity recovered from resting-state cortical dynamics largely overlaps with the structural connectivity (Honey et al. 2007; Zhou et al. 2013). In addition, cortical wave dynamics are often observed in the brain (Rubino et al. 2006; Muller et al. 2018). Theoretical studies indicate that these waves originate preferably from hub areas in the network (Roberts et al. 2019), and the emergence of the waves is influenced by the topology and connection distance of the network (Jirsa and Haken 1996). The topological structure of the brain network also highly correlates with specific brain functions (Jbabdi et al. 2013). Consequently, pathological perturbations to the brain structure will result in various brain disorders, as reviewed in (Fornito et al. 2015). For instance, in contrast to healthy controls, schizophrenia patients have an increased connection distance in their anatomically connected multimodal cortical network (Bassett et al. 2008). It is hypothesized that childhood-onset schizophrenia is induced by the overpruning of short-distance connections during the developmental stage (Feinberg 1983).

To quantitatively characterize the structure of brain networks, tools from graph theory and network science have been introduced into the neuroscience field (Bullmore and Sporns 2009; Bassett and Sporns 2017). Following the terminology of network science, neurons or brain regions are often described as nodes and the connections among them are described as edges. Subsequently, network characteristics including node degree distributions, clustering coefficients, shortest path lengths,

assortativity, and modularity have been calculated based on experimental measurements. It has been found that brain networks exhibit features of complex networks with highly connected hubs (Bullmore and Sporns 2012; van den Heuvel et al. 2012) and modularity (Meunier et al. 2010; Bullmore and Sporns 2012; Sporns and Betzel 2016). These network features are believed to facilitate functional integration and segregation of distinct brain regions (Young 1992; Hilgetag et al. 2000; Hilgetag and Kaiser 2004). In addition, brain networks have been identified with the small-world property characterized by small shortest path lengths and high clustering coefficients (Watts and Strogatz 1998; Bassett and Bullmore 2006; He et al. 2007), which presumably optimizes the complexity of brain functions meanwhile saving wiring costs (Bassett and Bullmore 2006).

In addition to the aforementioned rich topological features, brain networks also possess the geometrical feature of spatial embedding (Barthélemy 2018). This also imposes constraints on the network structure (Ramon-y-Cajal et al. 1996; Stiso and Bassett 2018). In fact, the network formation during brain development is largely determined by the chemical gradients of growth factors across space (Bayer and Altman 1987; Bullmore and Sporns 2012). As a consequence, neurons with similar functions tend to have more similar connection profiles than neurons with less similar functions (French and Pavlidis 2011; Rubinov et al. 2015). In addition, because of space limitation, the number of neurons as well as the length and cross-sectional diameter of axonal projections in brain networks are substantially restricted (Bullmore and Sporns 2012). Furthermore, the cost of establishing and maintaining axonal wiring connections increases with the wiring length of interneuronal connections (Chklovskii 2004). Under these constraints, a large number of connections in brain networks are observed to be local and short-distance (Hellwig 2000; Stepanyants et al. 2007).

As a basic structural characteristic of brain networks, the distribution of wiring length has been measured in recent experiments. In general, the wiring length distribution is observed to peak at a short-distance level with a long tail across multiple species (Kaiser et al. 2009; Betzel and Bassett 2018). This fact indicates that brain networks comprise a substantial amount of short-range connections with an admixture of long-range connections. The long-range connections increase the wiring cost, and in return for this, they presumably bring important functional benefits such as supporting efficient communication (Laughlin and Sejnowski 2003) and facilitating functional diversity (Betzel and Bassett 2018) in the brain. To further quantify the portion of long-range connections, the shape of wiring length distribution has been analyzed across species. In particular, the wiring probability as a function of distance between neurons in the neural network of *C. elegans* is found to be best fitted by a power-law distribution, and that in the neuronal network of rat visual cortex is found to be best fitted by a Gaussian distribution (Kaiser et al. 2009). In the interarea network of macaque, the dependence of wiring probability on distance has been reported as gamma (Kaiser et al. 2009) and exponentially distributed (Ercsey-Ravasz et al. 2013) in 2 independent studies, respectively. Using scaling theory, power-law distribution is theoretically proved to be the optimal solution of wiring length distribution under certain conditions (Karbowski 2001).

Based on experimental observations, computational models have been developed to capture the distribution of wiring length. In particular, generative models have been proposed to well fit the wiring length distributions of macaque and human brain networks, respectively (Ercsey-Ravasz et al. 2013; Song et al. 2014; Betzel et al. 2016). Yet these models often contain free parameters to be determined by fitting the network statistics. Accordingly, they are incapable of predicting the wiring length distribution without tuning the optimal parameter sets, thus impeding the understanding of the principle underlying the emergence of the wiring length distribution. Alternatively, optimization models suggest that the wiring length distribution of the macaque brain network is optimally determined from the tradeoff between wiring cost and functional efficiency (Chen et al. 2017). However, in contrast to the definition of wiring cost (Cherniak 1992; Chklovskii 2004), the definition of functional efficiency so far remains to be ambiguous. For example, the functional efficiency defined as the shortest path length or others in the optimization models (Chen et al. 2017) is arguable (Song et al. 2014; Betzel and Bassett 2018).

As a further step to understand the organizational principle of brain networks, the following questions need to be addressed: (1) What is the common feature of the wiring length distribution across different species, if any? (2) Is there a fundamental principle underlying the emergence of the wiring length distribution of a brain network? (3) How does the experimentally observed wiring length distribution emerge during network formation? (4) Are the experimentally observed wiring length distributions optimally designed for any brain function?

In this work, by quantifying the structural diversity of a brain network using the measure of Shannon's entropy (Shannon 1948; Rubinov and Sporns 2011; Chen et al. 2017), we show that the wiring length distribution across multiple species—including *Drosophila*, mouse, macaque, human, and *C. elegans*—follows the maximum entropy principle (MEP) under the constraints of (1) the spatial locations of brain areas or neurons and (2) the limited material resource described by average wiring length. This predictive framework is parameter free as all the information required by the 2 constraints can be explicitly determined from experimental measurements. In addition, by considering the stochasticity of axonal growth (Kaiser et al. 2009; Braitenberg and Schüz 2013), we propose a network formation procedure which is capable of reproducing the wiring length distribution for multiple species as observed in experiments, thereby implementing the MEP in a biologically plausible manner. To recover the detailed information of a brain network connectivity, we further develop a generative model by incorporating the cost-constrained MEP. For all the 5 species, we show that the network reconstructed by our generative model is more similar to the real network compared with those reconstructed by alternative generative models without accounting for the wiring entropy, that is, the entropy of the wiring length distribution of the network. Finally, we discuss the functional implications of the MEP, and show the predictability of the MEP for other transport networks beyond brain networks including the real-world flight course network, road network, and subway network etc.

Materials and Methods

Data Source

We analyze the brain network structure of *Drosophila*, mouse, macaque, human, and *C. elegans*. Based on experiments, the connections are measured among neurons for *C. elegans*, whereas the connections are measured among brain areas for the other species. In our analysis, we focus on the wiring length distribution of a network. Accordingly, we use the binary information

of the network connectivity, that is, the information of whether 2 neurons or brain areas are connected or not, although the networks per se are directed and weighted. The data we analyze are obtained from the sites described below.

Drosophila

The network connectivity for *Drosophila* brain was reconstructed based on the data in (Chiang et al. 2011), which is also available online in the FlyCircuit 1.2 database (http://www.flycircuit.tw). Labeled with green fluorescent protein, single neurons were imaged at high resolution, delineated from whole-brain 3D images and coregistered to a *Drosophila* female adult template brain. The mesoscopic map was partitioned into 49 local processing units (LPU) with distinct morphological and functional characteristics. LPUs were defined so as to contain their own population of local interneurons whose fibers were limited to that specific LPU. We focus our analysis on the 2106 connections among the 49 LPUs.

Mouse

The network connectivity for mouse brain was reconstructed based on tract-tracing data in (Oh et al. 2014), which is also available on the Allen Institute Mouse Brain Connectivity Atlas (http://connectivity.brain-map.org). To build the database, axonal projections of neurons were traced with enhanced green fluorescent protein-expressing adeno-associated viral vectors and imaged by high-throughput serial 2-photon tomography throughout the brain. The viral tracer projection patterns were reconstructed and registered to a common 3D reference space. Network areas were defined according to a custom parcellation based on the Allen Developing Mouse Brain Atlas. This parcellation contains 65 areas in each hemisphere, 9 of which were removed because they were not involved in any tract-tracing experiment. The resulting network contains 112 areas and 6542 connections.

Macaque

The network connectivity for macaque brain was reconstructed based on the online CoCoMac database (http://cocomac.g-node.org/main/index.php). The database covers connectivity data across literatures on tract-tracing experiments in macaque brain (Goldman-Rakic and Rakic 1991; Carmichael and Price 1994; Lewis and Essen 2000; Kötter 2004). Later analysis of the database provides a direct repository of spatial positions of 95 cortical areas and 2390 connections among areas, which are available on https://www.dynamic-connectome.org (Kaiser and Hilgetag 2006). Recently, the database has been further expanded to include 103 cortical areas and 2518 connections using a more detailed parcellation of the motor regions (Chen et al. 2013; Chen et al. 2017), which will be analyzed in our work.

Human

The human brain network we analyze is from (Betzel and Bassett 2018), which includes 128 cortical areas and 4736 connections. It was reconstructed from diffusion weighted magnetic resonance imaging, based on deterministic tractography algorithms. The data represent the composites of 30 human subjects.

C. elegans

The network connectivity for *C. elegans* was reconstructed from 2 online databases (https://www.wormatlas.org and https://www.dynamic-connectome.org). Both databases were based on the electron micrographs published in (White et al. 1986) and were updated with newly identified synapses. The first database was provided and analyzed in (Chen et al. 2006; Chen 2007; varshney et al. 2011), which incorporated additional synapses identified from other works (Durbin 1987; Hall and Russell 1991; Achacoso and Yamamoto 1992). The database includes 280 neurons, 6393 chemical synapses, 890 electrical junctions, and 1410 neuromuscular junctions. The chemical and electrical synapses are both considered as connections in our analysis. The second database was published in (Choe et al. 2004; Kaiser and Hilgetag 2006), which includes 277 neurons and 2105 synapses. The connectivity of neurons from these 2 databases do not fully overlap with each other. In our analysis, we use the intersection of neuron sets and the union of synapse sets in the 2 databases, which yields 277 neurons and 4758 connections for analysis. This network is referred to as the *C. elegans* global network. In addition, we reconstruct a *C. elegans* local network composed of neurons in the frontal area of the global network, which includes 169 neurons and 1331 connections. We use the information of the spatial positions of neurons provided by the second database. The spatial layout of the global and local networks is shown in Supplementary Figure S1.

Results

MEP Predicts the Wiring Length Distribution

The brain network in general consists of both short-range and long-range connections. It is evident that short-range connections require less material therefore substantially save the material cost. In contrast, long-range connections utilize more material and presumably benefit certain brain functions. However, the functional role of long-range connections remains to be fully elucidated, which impedes one to understand the spatial organizational principle of the brain network. Here we investigate the organizational principle from a different perspective. Rather than exploring the functional benefits of network structure, we investigate the question of whether there exists any universal structural characteristic that brain networks evolve to possess, as all functional benefits are supported by network structure. We are particularly interested in the wiring length distribution of brain networks, which reveals the portion of short-range and long-range connections that the brain invests resource to establish.

To address this question, we first analyze brain networks of 4 species—*Drosophila*, mouse, macaque, and human. The connections in these 4 networks are measured among brain areas (see Materials and Methods section for details). In addition, the wiring length d between 2 brain areas is measured by using the Euclidian distance (Betzel and Bassett 2018), and all the wiring lengths are partitioned into even bins $[d_i, .d_{i+1}), i = 1, 2, \ldots, k.$ to calculate the wiring length frequency distribution $p_i = P(d \in [d_i, .d_{i+1}))$. As shown in Fig. 1 and Supplementary Figure S2, the shapes of these distributions are dissimilar using either the same bin number or the same bin size. For example, the wiring length distribution for macaque is heavily skewed, whereas that for human is nearly symmetric. For the purpose of result demonstration, the number of bins is set to be $k = 30$ in Fig. 1 for processing data obtained from different species, yet the results

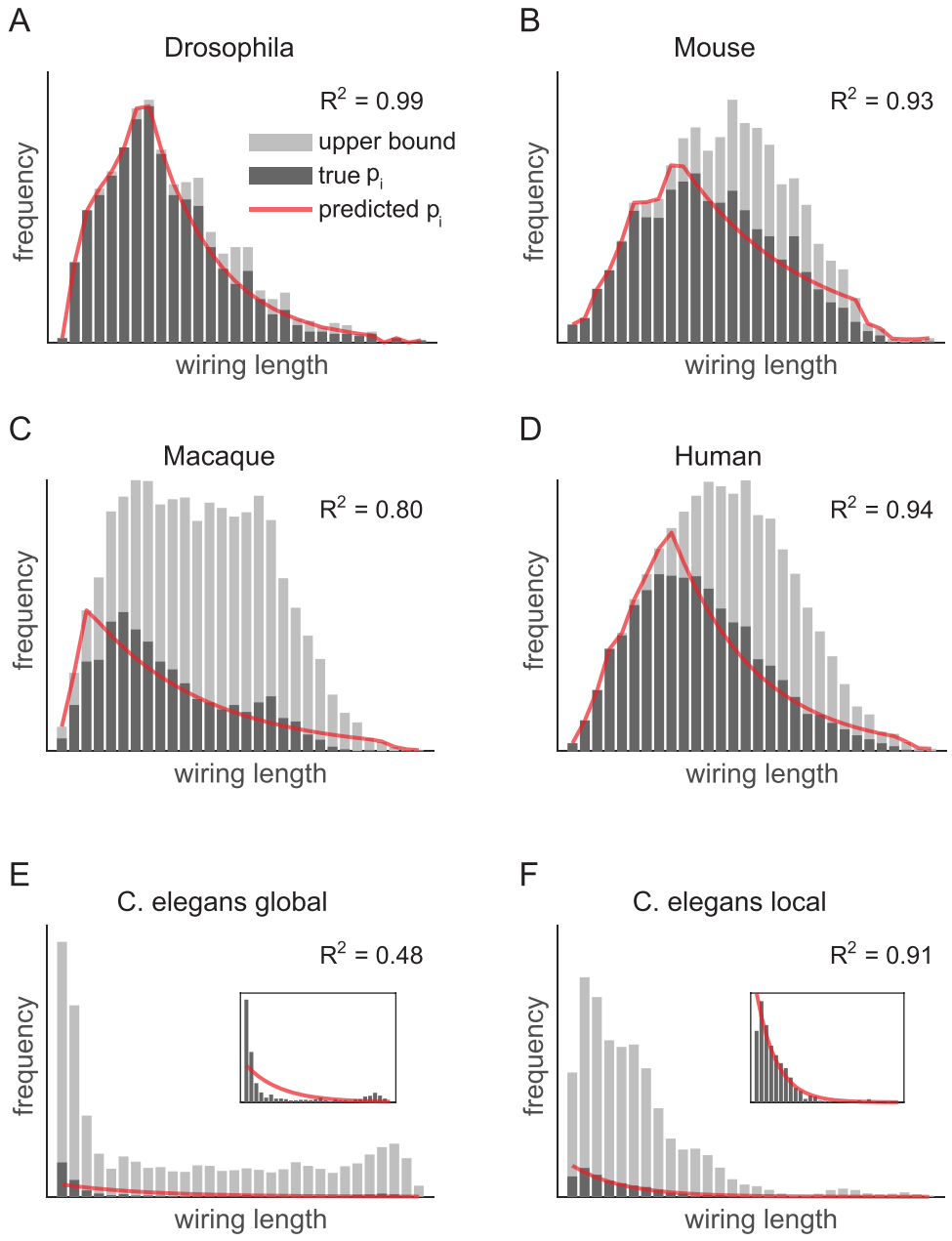

Figure 1. Wiring length distributions of brain networks across multiple species and their predictions by the maximum entropy principle. (A)–(D) are for brain networks of *Drosophila*, mouse, macaque, human, respectively. (E) and (F) are for the global and local neural networks of *C. elagans*, respectively. The insets of (E) and (F) are zooming in. In each panel, dark gray bars are the wiring length distribution measured from experiments. Light gray bars are the upper bound of the wiring length distribution given by the reference distribution defined in the main text. Red solid line is the wiring length distribution predicted by the maximum entropy principle (Eqs. 1–4). R^2 is calculated to evaluate the performance of the prediction. (A)–(F) share the same legend.

shown below are insensitive to the choice of bin number in a reasonable range (Supplementary Fig. S3). The dissimilarity among the wiring length distributions for different species is caused by at least 2 factors, that is, the locations of brain areas as the spatial constraint, and the total wiring length as the constraint of material cost.

To demonstrate the spatial constraint on a brain network, we first define the reference distribution as $\frac{N}{M}\ q_i$, where M is the number of connections in the real brain network, N is the number of connections in a corresponding fully connected brain network consisting of the same brain areas as the real brain network, and q_i is the wiring length distribution of the fully connected brain network. Note that the reference distribution is not necessarily a probability distribution because $\sum_i \frac{N}{M} \cdot q_i = \frac{N}{M} \neq 1$unless $M = N$, yet the reference distribution gives the upper bound of p_i. As shown in Fig. 1, the wiring length distribution p_i is always under the reference distribution for all networks, that is, $p_i \leq \frac{N}{M} \cdot q_i$. This is due to the fact that the number of connections with wiring length falling into the bin $[d_i, .d_{i+1})$, shall be no larger than the number of all available connections with wiring length

falling into the same bin, that is, $p_i \cdot M \leq q_i \cdot N$. Note that q_i—defined as the wiring length distribution of the fully connected brain network—is determined by the spatial locations of the brain areas, hence p_i is spatially constrained.

In addition, for all the 4 networks, we note that the rising part of the wiring length distribution p_i nearly overlaps with the rising part of the reference distribution. Their overlap indicates that the brain network exploits almost all the short-range connections that are available to form. This observation supports the hypothesis that the brain network tends to form short-range connections in order to save material cost. Furthermore, as shown in Fig. 1, for all the 4 networks, the decay part of the wiring length distribution p_i exhibits a substantial difference from their reference distribution. This observation suggests that the brain network chooses to form only a small portion of long-range connections instead of all of the available ones, which presumably results from the constraint of wiring resource.

Note that the constraints of spatial locations and material cost are not sufficient to determine the wiring length distribution. In fact, under the 2 constraints, it remains feasible for the brain network to form additional long-range connections in compensation for removing short-range connections while keeping the total material cost unchanged, and vice versa. Therefore, revealing the principle underlying the wiring length distribution is still an open question. It is hypothesized that the network structure is optimized for information processing functionally. However, the definition of functional efficiency of the brain remains ambiguous as mentioned previously. By focusing the network structure per se, here we hypothesize that the network structure is optimally diversified, and the MEP is an underlying rule to determine the network structure as discussed below.

Driven by this hypothesis, we first introduce the measure of Shannon's entropy to quantify the diversity of the network structure. The wiring entropy of a network is defined as $H = -\sum_{i=1}^{k} p_i \log(p_i)$, and is calculated for the 4 brain networks. As a reference, we estimate the upper and lower bounds of the wiring entropy that each brain network can achieve in the absence of any constraint. In principle, the upper bound of wiring entropy shall be obtained by exhaustively searching for all possible network configurations, that is, keeping network nodes the same as those in a given brain network meanwhile rewiring network edges in all possible ways, which is not feasible due to the extremely high computational cost. Alternatively, for each brain network, we construct an ensemble of 100 random networks by randomly connecting each pair of brain areas until the total number of connections reaches that of the original brain network. The largest entropy value of these random networks well approximates the upper bound of the brain wiring entropy (Supplementary Fig. S4). In addition, for each brain network, we construct a network by successively connecting the pair of brain areas with the smallest length until the total number of connections reaches that of the original brain network. The entropy value of this network approximates the lower bound of the brain wiring entropy. Subsequently, we find that all the 4 brain networks possess large wiring entropy close to the upper bound whereas the wiring entropy is substantially larger than the lower bound, as shown in Fig. 2. The large entropy of these brain networks across different species attributes to their broad wiring length distribution as an indicator of the structural diversity of these networks. On the other hand, as shown in Supplementary Figure S5, the material cost of these brain networks in most cases is significantly lower than that of the random networks, indicating that these brain networks are not fully random, and there is a trade-off balance between minimizing the material cost and maximizing the wiring entropy for the connectivity structure of real brain networks.

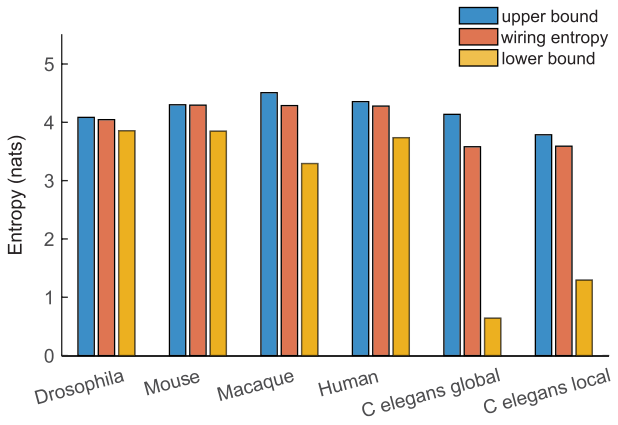

Figure 2. Wiring entropy of the 6 brain networks. Red bars correspond to the wiring entropy of *Drosophila*, mouse, macaque, human, the global and local networks of *C. elegans*. Blue and yellow bars are their upper and lower bounds, respectively. See text for the calculation of the upper bound and lower bound of wiring entropy.

Based on the above analysis of the wiring entropy, we next investigate the question of whether entropy maximization is sufficient to determine the wiring length distribution in addition to the constraints of spatial locations and material cost. We find that the wiring length distribution of all the 4 brain networks can be well predicted by the solution of the following optimization problem.

$$\text{maximize} - \sum_{i=1}^{k} p_i \log(p_i) \tag{1}$$

$$\text{subject to} \sum_{i=1}^{k} p_i = 1 \tag{2}$$

$$\sum_{i=1}^{k} p_i \cdot d_i \leq \bar{d} \tag{3}$$

$$p_i \leq \frac{N}{M} q_i \text{ for } i = 1, 2, \ldots, k \tag{4}$$

where Eq. 2 (normalization constraint) is the normalization condition for frequency p_i; Eq. 3 (material constraint) requires the average wiring length to be no larger than $\bar{d}$, which is measured as the average material cost in the brain network of each species; Eq. 4 (spatial constraint) requires that the number of connections with wiring length in the range $[d_i, d_{i+1})$cannot exceed the number of all available connections with wiring length in the same range. This optimization problem (Eqs. 1–4) is referred to as the MEP model. It is noticed that the MEP model is parameter free.

We use CVX Matlab software (Grant and Boyd 2008, 2014) as a convex optimization problem solver to find the global optimal solution of the MEP model for each of the 4 brain networks, that is, *Drosophila*, mouse, macaque, and human brain. As shown in Fig. 1A–D, the optimal solutions well overlap with the experimentally observed wiring length distributions for all the 4 brain networks. Further, R^2 is calculated to quantify the performance of the predictions—$R^2 = 0.99$ for *Drosophila* network, $R^2 = 0.93$ for mouse network, $R^2 = 0.80$ for macaque network, and $R^2 = 0.94$ for human network.

In addition to analyzing the 4 brain networks with connections measured among brain regions, we have also analyzed the *C. elegans* network in which connections are measured between neurons. Fig. 2 shows that the wiring entropy of *C. elegans* also approaches to its upper bound while is substantially larger than its lower bound. In addition, as shown in Fig. 1E, the prediction of the wiring length distribution from the MEP fits the observed distribution moderately well with $R^2 = 0.48$. However, the performance of the prediction can be substantially improved in Fig. 1F with $R^2 = 0.91$ if considering a local network located in the frontal area of the *C. elegans*. It is speculated that the moderate prediction performance of the *C. elegans* global network may attribute to the fact that the alignment of neurons in the global network is approximately 1D as shown in Supplementary Figure S1, which may weaken the predictive power of the MEP.

We point out that the constraint of material cost in the MEP model is set to be no greater than a constant $\bar{d}$ measured from experiment, which allows a network to use less material than the real one measured in experiment. This constraint together with the other 2 constraints create a large feasible region of the MEP model, that is, there are a large number of possible solutions that satisfy the constraints. However, the objective function of entropy maximization picks out only 1 solution that turns out to be consistent with the wiring length distribution observed in the real brain network, indicating that entropy maximization may be a potential principle of brain network organization.

Biological Implementation of the MEP

The MEP model provides a principle of the wiring distribution of brain networks, yet it remains unclear on the biological implementation underlying this principle during the stage of network wiring formation. Theoretical and experimental works have shown that many factors are involved in the determination of the network structure including spatial distance, molecular gradients (Bayer and Altman 1987; Bullmore and Sporns 2012), neurogenesis (Picco et al. 2018; Goulas et al. 2019), developmental time window (Goulas et al. 2019), cortical expansion (Beul et al. 2018), stochastic axon growth (Binzegger et al. 2004; Kaiser et al. 2009) etc. Under the tight constraints of these factors, the brain network connectivity is largely determined. However, it remains interesting to address the issue that, among all these factors, what the essential subset of factors are, if any, to determine the wiring length distribution observed in experiments. As wiring entropy in the MEP model depicts the randomness of network structure, here we investigate if random axon growth during network development is sufficient to give rise to the observed wiring length distribution, with a few constraints derived from real brain network.

Fig. 3A–D illustrates a process of network formation by stochastic axonal growth, which is referred to as the random growth model below. In this process, the locations of all brain areas are embedded in the geometric space, and the distance between each pair of brain areas is set to be identical to that measured in experiment. Initially all brain areas are disconnected. A bunch of axons from each area start to grow out with a constant speed toward random directions in the 3D space. The growth of an axon from one area terminates with certain probability once the axon reaches the vicinity of another area if the number of connections to the target area is not saturated yet (the saturation condition of connections will be discussed below). After sufficiently long simulation time, axons that fail to connect 2 areas will be pruned. To avoid the emergence of super rich hubs with unrealistically large number of degrees, each area is set to have a limited number of axons it can receive. In our simulations, the limited capacity for each area is set to equal the actual connection degree of the area. In addition, the radius of the "touching sphere" for each area is set to be identical, and this parameter is optimally chosen such that the total number of connections approximately equals that of the real brain network. Additional stochasticity is introduced by setting a failure probability of connection formation when an axon reaches the "touching sphere" of an area. If the failure of connection formation happens, the axon will continue to grow toward distal area, which increases the chance of forming long-range connections. The values of these biological parameters, including the number of outgrowing axons per area, the speed of axonal growth, the radius of the "touching sphere", and the failure probability of forming a new connection are listed in Supplementary Table S1. As shown in Fig. 3E–J, the random growth model well reproduces the wiring length distribution for all the brain networks across the 5 species, although the reproducing of the wiring length distribution for the *C. elegans* global network is not as good as that in other cases. The random growth model does not consider the maximization of wiring entropy as a priori, while it reproduces the wiring length distribution of the brain networks as an emergent phenomenon previously predicted by the MEP model. This result indicates that stochastic axonal growth may serve as a crucial factor that implements the MEP.

It is worth pointing out that, without accounting for other important factors related to network formation, this network growth model does not reflect the real network formation process, and the resultant network becomes stochastic rather than deterministic. Hence the detailed structure of the resultant network can be different from the true one. However, the true network can be viewed as a particular realization of the network ensembles generated by the network growth model, which will be uniquely determined by taking into account additional factors.

MEP Contributes to Network Connectivity and Various Statistical Properties

We further address the question of whether the principle of maximum entropy contributes to additional properties of network structure besides the wiring length distribution, such as network connectivity, clustering coefficient, and modular structure.

The MEP model (Eqs. 1–4) suggests that the structure of the brain network results from the balance between the minimization of material cost and the maximization of wiring entropy when the network is embedded in the geometrical space. According to this, we propose a generative model with the MEP (Eqs. 1–4) incorporated, which allows one to recover the detailed connectivity of the brain network. In the model, the spatial locations and the connectivity degrees of brain areas are given from the real brain network we attempt to reconstruct, and the material cost is calculated proportional to the Euclidian distance between each pair of brain areas. To recover the network connectivity and statistics, we initialize the network by disconnecting all the areas, that is, there is no connection in the initial network thus each area has a 0 degree of connection. We then create a candidate list to include all the areas whose current degree is less than the target degree given by the degree sequence measured from experiments. Initially,

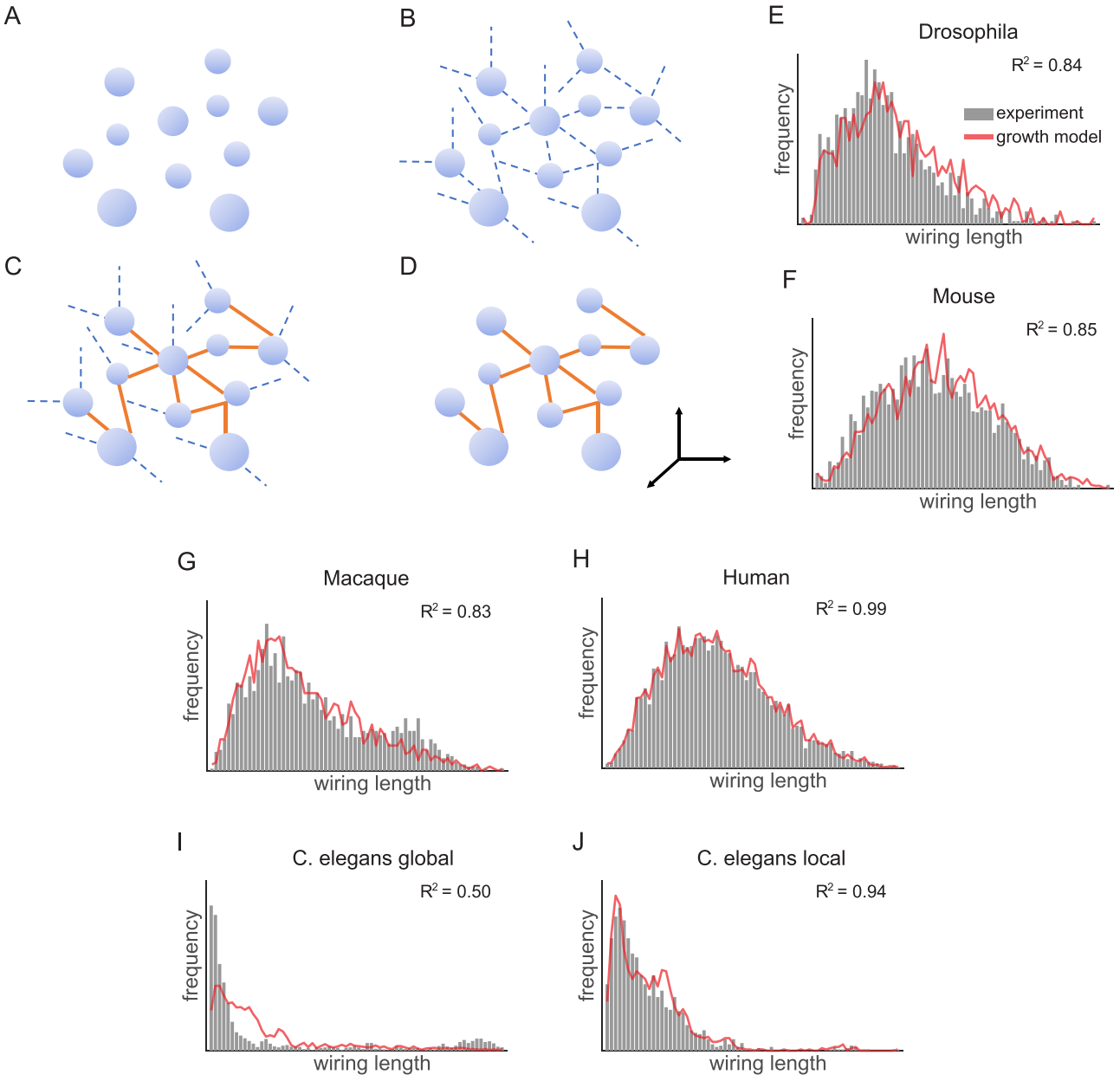

Figure 3. Random growth model reproduces the wiring length distributions of brain networks across multiple species. (A)–(D) Schematic illustration of the random growth process. (A) The initial state of a network with all brain areas disconnected. Each brain area is indicated as a dot in the 3D space with its coordinates measured from the experiments. Blue spheres are the "touching sphere" of each brain area. (B) The random growth stage. A bunch of axons (dash blue lines) from each brain area start to grow out with a constant speed toward random directions. (C) The connection formation stage. Connections are formed (orange lines) with a certain probability when growing axons (dash blue lines) fall into the touching sphere of another brain area that has not been fully occupied yet. (D) The pruning stage. Networks are formed by finally pruning axons that fail to connect 2 brain areas. (E)–(J) The wiring length distributions of the brain networks for *Drosophila*, mouse, macaque, human, the global and local networks of *C. elagans*, respectively. The gray bars are from experimental measurement, and the red curves are from the simulations of stochastic axonal growth.

all the areas' ID is in the candidate list because there is no connection in the network. We next introduce an objective function $F = H - \lambda\bar{d}$ to determine whether a selected pair of brain areas at each step should be connected or not, where H is the wiring entropy, $\bar{d}$ is the material cost or the average wiring length of the current network, and λ is a parameter that scales the relative contribution between wiring entropy and material cost. In each step of connection generation, we utilize the greedy searching strategy: (1) For each area V_i in the candidate list, hypothetically connect it to another area V_j in the candidate list whose current degree has the largest difference from its target degree. (2) For each pair of V_i and V_j, compute the objective function F after adding the hypothetical connection between V_i and V_j. (3) Select the pair of V_i and V_j to connect which corresponds to the largest F. (4) Update the degree of V_i and V_j from K_i and K_j to K_i+1 and $K_j + 1$, and update the candidate list by removing V_i or V_j if K_i or K_j reaches the real degree value of area V_i or V_j as observed in

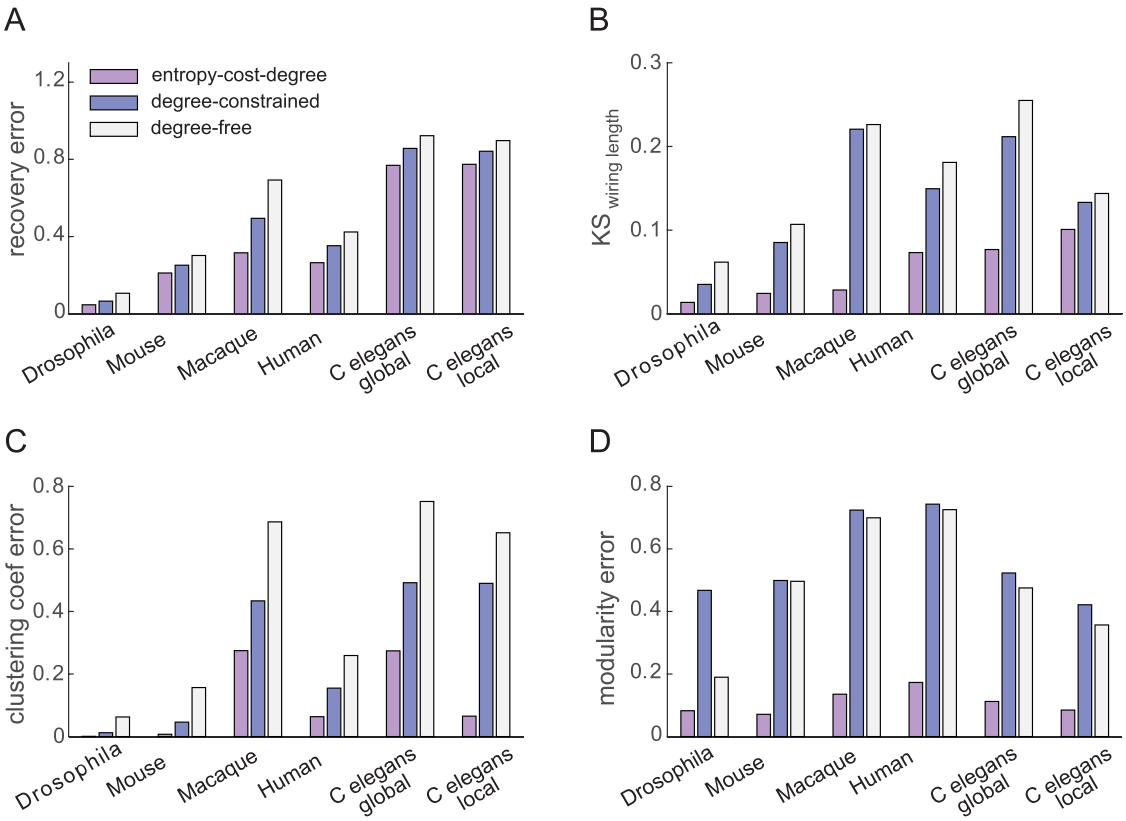

Figure 4. Performance of the generative models on the prediction of network structural properties for the 5 species. (A) Recovery error. (B) The distance between the wiring length distribution measured in experiment and that recovered by the generative models quantified by the Kolmogorov–Smirnov statistic. (C) and (D) are the absolute values of the relative error of the recovered real network's clustering coefficient and modularity factors, respectively. (A)–(D) share the same legend shown in (A). The values of λ in the generative models are chosen as 113 for *C. elegans* global network, 339 for *C. elegans* local network, 121 for *Drosophila* network, 7.91 for mouse network, 0.187 for macaque network, and 0.494 for human network (in the unit of mm^{-1}), based on the optimal performance of network connectivity reconstruction of the generative models.

experiment. (5) Repeat the above steps until the candidate list becomes empty. We refer this model to as the entropy-cost-degree (ECD) model. The ECD model provides more information than the MEP model (Eqs. 1–4), that is, the additional information of network connectivity thereafter statistical properties beyond the wiring length distribution. Therefore, the ECD model allows us to investigate the role of the MEP in determining network structure and property.

Note that, in addition to incorporating the MEP, the ECD model also incorporates the extra information of connectivity degree of brain areas (or neurons in the *C. elegans* network), that is, the connectivity degree shall be identical to that measured in the real brain network. To substantiate the unique role of the MEP on the determination of network structure, we further develop 2 alternative generative models for comparison. In the first model, in each step of connection generation, we randomly connect a pair of areas only under the constraint of degree sequence rather than optimizing *F*. The reconstructed network by this model has the same degree sequence as the real brain network. The model is referred to as the degree-constrained model. The degree-constrained model removes the influence of the MEP on network structure while only accounts for the contribution of degree information to the determination of network structure. Accordingly, the improved performance from the degree-constrained model to the ECD model attributes to the MEP. In addition, we propose a second generative model that further removes the information of degree sequence. In this model, a pair of brain areas is randomly chosen to be connected at each step until the total number of connections equal that in the real brain network. This model is referred to as the degree-free model. Accordingly, the improved performance from the degree-free model to the degree-constrained model attributes to the additional information of degree sequence.

We first assess the performance of the generative models on the recovery of the network connectivity, which is evaluated by the recovery rate r_{rec} defined as the ratio of the number of successfully recovered connections by a generative model to the total number of existing connections in the real network, and the recovery error as $1 - r_{rec}$. As shown in Fig. 4A, for the brain networks of *Drosophila*, mouse, macaque, and human, the recovery error of the ECD model is below 35%. In contrast, for the global and local networks of *C. elegans*, the recovery error of the ECD model is as large as about 80%. The large recovery error of the network connectivity for *C. elegans* results from the sparsity of the network connections. In the sparse network of *C. elegans*, all the existing connections with a fixed length are only a small portion of the total available connections with identical length. Therefore, there exists a large number of network configurations that share similar entropy and cost to the real *C. elegans* network, which gives rise to the large recovery error. Fig. 4A shows that the recovered connectivity by the ECD model for all the

5 species is consistently and significantly more accurate than that of the degree-free model. This result indicates that network connectivity recovered by the ECD model cannot be achieved by random guess. Therefore, the MEP as well as degree sequence constraint plays important roles in the recovery of the network connectivity. To demonstrate the relative contribution of the MEP and the constraint of degree sequence in the ECD model to the recovery of network connectivity, the performance of the ECD model is compared with the degree-constrained model. It is noted that the recovery error increases once the maximum entropy condition is removed, indicating that the MEP plays a unique role in determining network structure. The increase of recovery error from the ECD model to the degree-constrained model is about 6.98% ± 4.76% (mean ± standard deviation for 6 networks across 5 species). In addition, the recovery error further increases from the degree-constrained model to the degree-free model by 8.02% ± 5.89% in a consistent way for all the 5 species, demonstrating that degree sequence is also informative for the reconstruction of network connectivity.

We further show that maximizing wiring entropy in the ECD model also improves the recovery of network statistical properties including wiring length distribution, clustering coefficient, and modularity factor. We first investigate the performance of the generative models on recovering wiring length distribution evaluated by the Kolmogorov–Smirnov(K–S) statistics (Kolmogorov 1933; Smirnov 1948). By its definition, given a measured wiring length distribution and its prediction from one of the generative models, the smaller the K–S statistic value is, the closer the predicted wiring length distribution is to the measured distribution. Therefore, a smaller value of the K–S statistic indicates a better prediction from a generative model. As shown in Fig. 4*B*, among the 3 generative models, the ECD model best predicts the wiring length distribution of the brain networks for all the 5 species, and the performance drops by removing the constraint of the MEP (i.e., the degree-constrained model), consistent with the previous result that the MEP (Eqs. 1–4) well predicts the wiring length distributions. Similar hierarchy of model performance on the recovery of clustering coefficient (Watts and Strogatz 1998) and modularity factor (Newman 2006) of the brain networks are shown in Fig. 4*C* and *D*, respectively. The ECD model that accounts for wiring entropy always outperforms the other 2 generative models without considering wiring entropy, particularly for the recovery of network modular structure. The successful recovery of the feature of network modularity by the ECD model is further demonstrated in Fig. 5, which clearly shows the effectiveness of the ECD model in contrast to the degree-constrained model and the degree-free model.

Discussion

In this work, we have shown that the wiring length distributions of brain networks across multiple species—including *Drosophila*, mouse, macaque, human, and *C. elegans*—share the feature of large wiring entropy. These distributions have been well predicted by maximizing the entropy of wiring length under the constraints of limited wiring material and the spatial locations of neurons or brain areas. Mathematically equivalent, the connectivity of brain networks is largely determined by the trade-off balance between maximizing wiring entropy and minimizing wiring cost. In addition, we have proposed a process of random axonal growth to reproduce wiring length distributions for the 5 species as measured in experiments, thereby implementing the MEP in a biologically plausible manner. We have further developed a generative model incorporating the MEP, that is, the ECD model. We have shown that the ECD model significantly improves the recovery rate and other network statistics compared with alternative models without accounting for entropy, confirming that entropy maximization involves in determining the structure of brain networks. Our work implies that the connectivity in brain networks evolves to be structurally diversified to support its complex functions.

Network functions in general are realized by its dynamics, which can be substantially influenced by network structure (Honey et al. 2010). In this work, we focus on the network structure per se and ask the question of what structural features the brain network optimally evolves to possess under certain constraints. This distinguishes our work from previous works attempting to understand network structure from the viewpoint of functional benefits that in general are not well defined yet (Linsker 1988; Laughlin and Sejnowski 2003; Antonopoulos et al. 2015; Toker and Sommer 2019). In addition, our work identifies a concise yet effective principle of maximum entropy that may underly the wiring length distribution of networks both at the macroscale areal level and at the microscale neuronal level across multiple species from invertebrate to vertebrate. Without introducing extra tuning parameters, the accurate prediction of the wiring length distribution (with $R^2 > 0.9$ for most cases) indicates the universality of the MEP. Furthermore, our work investigates the structure of brain networks from multiple comprehensive angles—from theoretical principle to biological implementation and to phenomenological generative model. All these aspects are unified by the principle of maximum entropy, hence systematically establishes the relation between different theoretical approaches toward understanding network structure. This framework is expected to be generalizable by incorporating more biological constraints into it.

Previous works suggest that one of the functional benefits of brain information processing can be evaluated by the average shortest path (ASP) of the network (Watts and Strogatz 1998), which reflects the communication speed as the time it takes a neuronal signal to transmit from one area to another area on average (Bullmore and Sporns 2012). As demonstrated in Supplementary Figure S6, in an idealized brain network with a ring structure, we have shown using theoretical analysis that large wiring entropy or structural diversity corresponds to small ASP. In addition, we have examined the data of the real brain networks to investigate the relation between wiring entropy and ASP. It is noticed that the real brain network deviates from the idealized brain network in that the layout of the brain areas or neurons are not spatially uniform. Therefore, for each brain network of the 5 species, we first construct a corresponding approximately "spatially-regular" network by having each area connecting with a fixed number of spatially nearest neighboring areas. The number of connections is approximately identical for each area and is determined by the way such that the total number of connections in the spatially-regular network is the same as the real brain network. Because most connection lengths are short, the wiring length distribution of this network is narrowly peaked. Accordingly, the wiring entropy is small. We label the false positive (FP) connections and false negative (FN) connections in the spatially-regular network by comparing it with the real network. We then correct these connections step by step. In each step, we remove a pair of connection from the FP pool and add a pair of connection from the FN

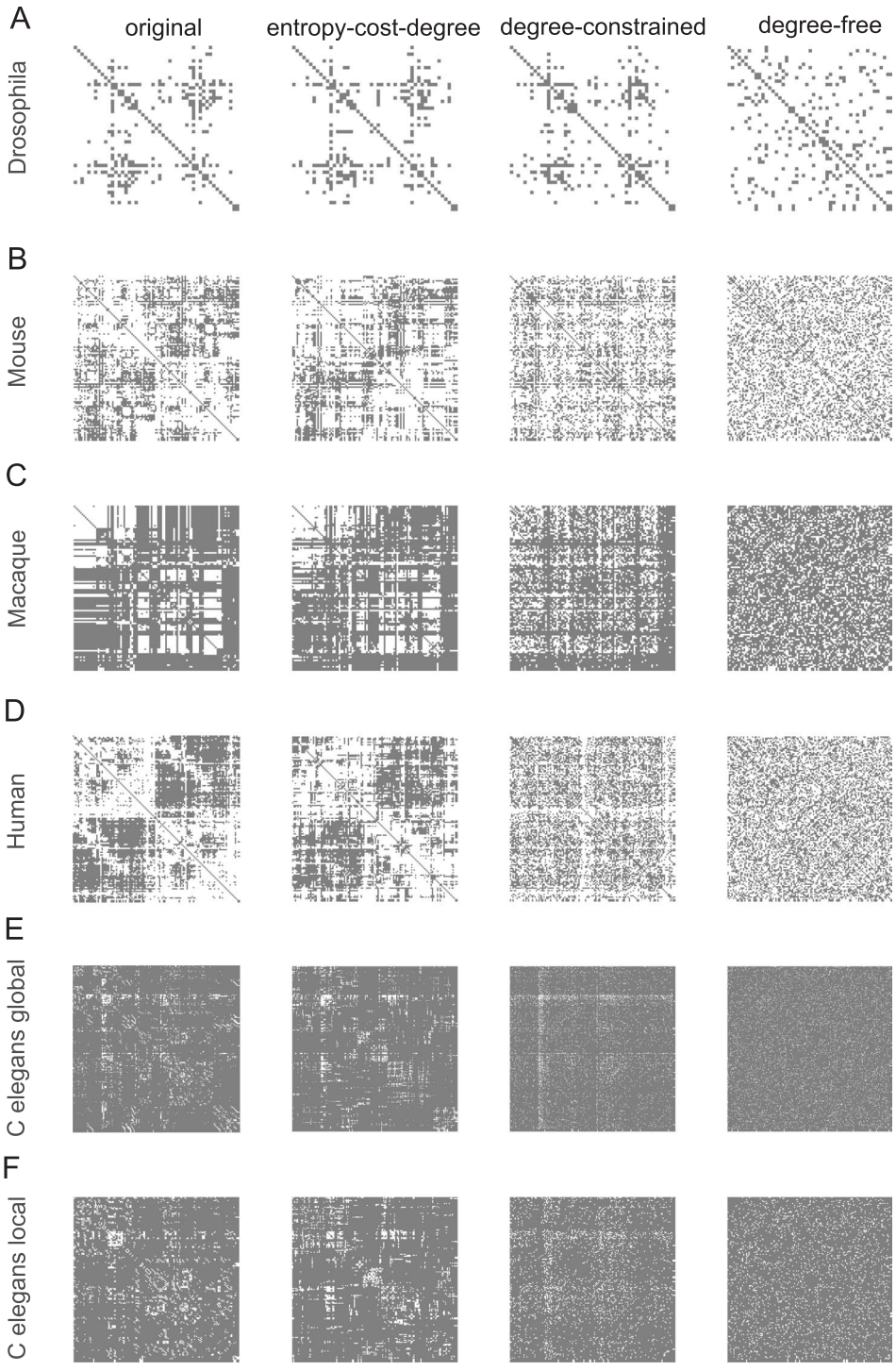

Figure 5. Reconstruction of network connectivity from the generative models. (A) *Drosophila* network. (B) Mouse network. (C) Macaque network. (D) Human network. (E) Global network of *C. elegans*. (F) Local network of *C. elegans*. In each panel, the connectivity matrices recovered from the ECD model, the degree-constrained model, and the degree-free model are compared with the connectivity matrix of the real brain network. The ECD model well recovers the modular structure of the real network, whereas other models fail to recover it.

pool. Both pairs of connections are selected to have the shortest length in their pools respectively. Entropy and ASP are calculated throughout the correction steps. After a finite number of steps, the network will be corrected to the real network. As shown in Fig. 6, except for *Drosophila* and mouse, all the brain networks show the strong negative correlation between wiring entropy and ASP—the entropy increases whereas the ASP decreases as the correction continues, suggesting that the maximization of wiring entropy benefits communication efficiency in these networks.

In contrast, for the *Drosophila* and mouse networks, as they evolve from spatially-regular to the real one, wiring entropy

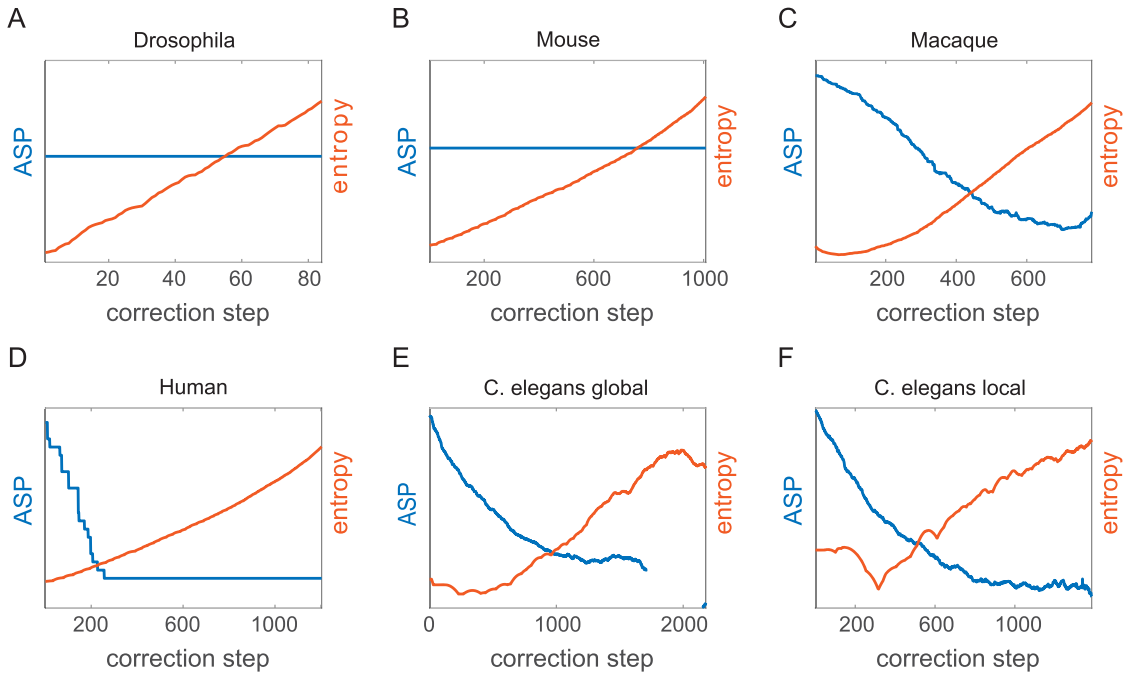

Figure 6. Negative correlation between wiring entropy and ASP for brain networks of the 5 species. (A) *Drosophila* network. (B) Mouse network. (C) Macaque network. (D) Human network. (E) Global network of *C. elegans*. (F) Local network of *C. elegans*. The black curve in (E) is cut at the correction step about 1700 when the network becomes disconnected.

increases whereas the ASP remains constant. The insensitivity of the ASP to network connectivity results from the fact that the 2 networks are densely connected, thus the ASP is small and does not change much during correction steps in the presence of a large amount of connections. The 2 exception cases of the *Drosophila* and mouse networks indicate that the maximization of wiring entropy can be a more general principle than the minimization of ASP under the constraint of limited material resource. As shown in Fig. 6, for brain networks of *Drosophila* and mouse, the optimal network structure with minimal ASP and material cost shall be the spatially-regular network rather than the real network. In addition, for the human brain network, the optimal network structure exists in the middle of the correction step, which is also different from the real network. In these networks, the maximization of entropy may have other functional implications, for instance, enhancing functional diversity (Betzel and Bassett 2018) or robustness (Demetrius and Manke 2005) of the network. The diverse wiring length distribution may also provide a broad spectrum of conduction delays of action potential and support a rich pool of neural dynamics, which echoes the previous theoretical studies about the temporal coding of spikes in the neural network (Izhikevich 2006). All these speculations require future investigations.

It is undeniable that, during the developmental stage of each individual organism, the formation of the macroscale structure of brain networks is largely determined by genetic factors rather than being random, which has been studied in many previous works (Bullmore and Sporns 2012; Beul et al. 2018; Picco et al. 2018; Goulas et al. 2019). Accordingly, the variability of macroscale brain connectivity across individuals is relatively small. Therefore, the random growth process we proposed does not fully reflect the real network formation process. However, the true network can be viewed as a particular realization in the network ensembles, which will be uniquely determined by taking into account more biological factors such as molecular gradients, neurogenesis, cortical expansion etc. In addition, the random growth model may play a crucial role during the formation of the microscale structure of neuronal networks in which randomness is strongly involved.

Although the main focus of this work is on brain networks, the MEP can be applied to other transport networks beyond brain networks. To demonstrate this, we have examined the networks of real-world subway, flight course, and road from different countries and countries. As shown in Supplementary Table S2, under the constraints of limited wiring material and the spatial locations of nodes, the wiring length distributions of these networks can also be well predicted by the MEP model. The diversity of network structures is supposed to benefit the efficiency of traffic transport in these networks.

In our work, we have also confirmed that material cost has a crucial impact on network structure (Bullmore and Sporns 2012). This is demonstrated in the objective function in the ECD model $F = H - \lambda \bar{d}$, where H is the wiring entropy and $\bar{d}$ is the average wiring length. The parameter λ scales the relative importance between the 2 quantities, and the optimal value of λ that leads to the most accurate network reconstruction is significantly nonzero in general, indicating the importance of the material cost in determining network connectivity. If we view λ as the cost per unit length, as the cost increases, network structure will change accordingly. For instance, as shown in Supplementary Figure S7, the networks reconstructed under various λ have distinct clustering coefficients. The larger the λ is, the more expensive the material cost is. In Supplementary Figure S7, the clustering coefficient has an overall increase under larger material cost with exception at certain λ value. Interestingly, by aligning the best-performance λ value

with the experimentally identified network clustering coefficient, we find that the peaks of the clustering coefficient value across species lie around the best reach of our generative model.

Many algorithms have been proposed for reconstructing neural networks and have achieved good performances (Betzel et al. 2016; Chen et al. 2017). Yet it remains challenging to fully recover the connectivity of a brain network. One challenge lies in the huge space of network configurations. In general, the reconstruction algorithms start with neurons or areas being disconnected. Connections are added gradually based on certain optimization rules. For a network of N nodes, the potential network configurations can be as many as $N!$, which is about 10^{164} for the macaque cortical network. Therefore, exhaustive searching is impossible to be realized. The ECD model partially solves the problem by achieving an accuracy of recovery rate 68% in macaque cortical network, which is comparable with earlier algorithms (Betzel et al. 2016; Chen et al. 2017). Another challenge lies in the identification of factors that determine network structure. The structure of brain networks is determined by various factors, for instance, spatial geometry, gene expression, chemical gradients of growth factors, randomness of axonal growth, energy consumption, and material cost. Here we have shown that the network statistics of wiring length distribution is largely determined by the spatial constraint and material cost constraint when maximizing wiring entropy and realized by random axonal growth. However, these factors are insufficient to accurately recover detailed network connectivity, as demonstrated by the performance of the ECD model. Therefore, to incorporate more factors in the generative model can be a future direction to understand network connectivity. For instance, the ECD model can be further modified by taking into account the direction and weight of connections in the future study.

Supplementary Material

Supplementary material is available at *Cerebral Cortex* online.

Funding

National Key R&D Program of China 2019YFA0709503, Shanghai Municipal Science and Technology Major Project 2021SHZDZX0102 (S.L., D.Z.); National Natural Science Foundation of China Grants 11901388, Shanghai Sailing Program 19YF1421400, Shanghai Chengguang program (S.L.); and Natural Science Foundation of China Grants 12071287, 11671259, 11722107 (D.Z.), and Student Innovation Center at Shanghai Jiao Tong University.

Notes

The authors thank Richard Betzel for sharing the data of the *Drosophila*, mouse, and human brain network, and thank Christopher J. Honey, Yuhan Chen, and Yanyang Xiao for helpful discussions. *Conflict of Interest*: None declared.

References

Achacoso TB, Yamamoto WS. 1992. *Ay's Neuroanatomy of C. elegans for computation*. Boca Raton, FL: CRC Press.

Antonopoulos CG, et al. 2015. Do brain networks evolve by maximizing their information flow capacity? *PLoS Comput Biol*. 11(8):1004372.

Barthélemy M. 2018. *Encyclopedia of social network analysis and mining*. New York, NY: Springer.

Bassett DS, Bullmore ED. 2006. Small-world brain networks. *Neuroscientist*. 12(6):512–523.

Bassett DS, Sporns O. 2017. Network neuroscience. *Nat Neurosci*. 20(3):353.

Bassett DS, Bullmore E, Verchinski BA, Mattay VS, Weinberger DR, Meyer-Lindenberg A. 2008. Hierarchical organization of human cortical networks in health and schizophrenia. *J Neurosci*. 28(37):9239–9248.

Bayer SA, Altman J. 1987. Directions in neurogenetic gradients and patterns of anatomical connections in the telencephalon. *Prog Neurobiol*. 29(1):57–106.

Betzel RF, Bassett DS. 2018. Specificity and robustness of long-distance connections in weighted, interareal connectomes. *Proc Natl Acad Sci USA*. 115(21):4880–4889.

Betzel RF, Avena-Koenigsberger A, Goñi J, He Y, de Reus MA, Griffa A, Vértes PE, Mišic B, Thiran JP, Hagmann P, et al. 2016. Generative models of the human connectome. *Neuroimage*. 124:1054–1064.

Beul SF, Goulas A, Hilgetag CC. 2018. Comprehensive computational modelling of the development of mammalian cortical connectivity underlying an architectonic type principle. *PLoS Comput Biol*. 14(11):e1006550.

Binzegger T, Douglas RJ, Martin KAC. 2004. A quantitative map of the circuit of cat primary visual cortex. *J Neurosci*. 24(39):8441–8453.

Braitenberg V, Schüz A. 2013. *Cortex: statistics and geometry of neuronal connectivity*. Berlin; Heidelberg; New York, NY: Springer Science & Business Media.

Bullmore E, Sporns O. 2009. Complex brain networks: graph theoretical analysis of structural and functional systems. *Nat Rev Neurosci*. 10(3):186.

Bullmore E, Sporns O. 2012. The economy of brain network organization. *Nat Rev Neurosci*. 13(5):336.

Carmichael ST, Price JL. 1994. Architectonic subdivision of the orbital and medial prefrontal cortex in the macaque monkey. *J Comp Neurol*. 346(3):366–402.

Chen BL. 2007. *Neuronal network of C. elegans: from anatomy to behavior*. In: *PhD thesis*. Cold Spring Harbor Laboratory.

Chen BL, Hall DH, Chklovskii DB. 2006. Wiring optimization can relate neuronal structure and function. *Proc Natl Acad Sci USA*. 103(12):4723–4728.

Chen Y, et al. 2013. Trade-off between multiple constraints enables simultaneous formation of modules and hubs in neural systems. *PLoS Comp Biol*. 9(3):1–20.

Chen Y, et al. 2017. Features of spatial and functional segregation and integration of the primate connectome revealed by trade-off between wiring cost and efficiency. *PLoS Comp Biol*. 13(9):e1005776.

Cherniak C. 1992. Local optimization of neuron arbors. *Biol Cybern*. 66(6):503–510.

Chiang A-S, Lin CY, Chuang CC, Chang HM, Hsieh CH, Yeh CW, Shih CT, Wu JJ, Wang GT, Chen YC, et al. 2011. Three-dimensional reconstruction of brain-wide wiring networks in drosophila at single-cell resolution. *Curr Biol*. 21(1):1–11.

Chklovskii DB. 2004. Exact solution for the optimal neuronal layout problem. *Neural Comput*. 16(10):2067–2078.

Choe Y, McCormick BH, Koh W. 2004. Network connectivity analysis on the temporally augmented C. elegans web: a pilot study. *Abstr Soc Neurosci*. 30:921–929.

Demetrius L, Manke T. 2005. Robustness and network evolution—an entropic principle. *Physica A*. 346(3–4):682–696.

Durbin RM. 1987. Studies on the development and organisation of the nervous system Of Caenorhabditis Elegans. In: *Phd thesis*. Accessed at https://www.wormatlas.org.

Ercsey-Ravasz M, Markov NT, Lamy C, van Essen DC, Knoblauch K, Toroczkai Z, Kennedy H. 2013. A predictive network model of cerebral cortical connectivity based on a distance rule. *Neuron*. 80(1):184–197.

Feinberg I. 1983. Schizophrenia: caused by a fault in programmed synaptic elimination during adolescence? *J Psychiatr Res*. 17(4):319–334.

Fornito A, Zalesky A, Breakspear M. 2015. The connectomics of brain disorders. *Nat Rev Neurosci*. 16(3):159.

French L, Pavlidis P. 2011. Relationships between gene expression and brain wiring in the adult rodent brain. *PLoS Comp Biol*. 7(1):e1001049.

Goulas A, Betzel RF, Hilgetag CC. 2019. Spatiotemporal ontogeny of brain wiring. *Sci Adv*. 5(6):eaav9694.

Grant M, Boyd S. 2008. Graph implementations for nonsmooth convex programs. In: Blondel V, Boyd S, Kimura H, editors. *Recent advances in learning and control*. London (UK): Springer.

Grant M, Boyd S. 2014. *CVX: Matlab software for disciplined convex programming*, version 2.1. Accessed at http://cvxr.com/.

Hall DH, Russell RL. 1991. The posterior nervous system of the nematode Caenorhabditis elegans: serial reconstruction of identified neurons and complete pattern of synaptic interactions. *J Neurosci*. 11(1):1–22.

He Y, Chen ZJ, Evans AC. 2007. Small-world anatomical networks in the human brain revealed by cortical thickness from MRI. *Cereb Cortex*. 17(10):2407–2419.

Hellwig B. 2000. A quantitative analysis of the local connectivity between pyramidal neurons in layers 2/3 of the rat visual cortex. *Biol Cybern*. 82(2):111–121.

Hilgetag CC, Kaiser M. 2004. Clustered organization of cortical connectivity. *Neuroinformatics*. 2(3):353–360.

Hilgetag CC, Burns GAPC, O'Neill MA, Scannell JW, Young MP. 2000. Anatomical connectivity defines the organization of clusters of cortical areas in the macaque and the cat. *Philos Trans R Soc Lond B Biol Sci*. 355(1393):91–110.

Honey CJ, Thivierge J-P, Sporns O. 2010. Can structure predict function in the human brain? *Neuroimage*. 52(3):766–776.

Honey CJ, Kotter R, Breakspear M, Sporns O. 2007. Network structure of cerebral cortex shapes functional connectivity on multiple time scales. *Proc Natl Acad Sci USA*. 104(24):10240–10245.

Izhikevich EM. 2006. Polychronization: computation with spikes. *Neural Comput*. 18(2):245–282.

Jbabdi S, Sotiropoulos SN, Behrens TE. 2013. The topographic connectome. *Curr Opin Neurobiol*. 23(2):207–215.

Jirsa VK, Haken H. 1996. Field theory of electromagnetic brain activity. *Phys Rev Lett*. 77(5):960.

Kaiser M, Hilgetag CC. 2006. Nonoptimal component placement, but short processing paths, due to long-distance projections in neural systems. *PLoS Comp Biol*. 2(7):95.

Kaiser M, Hilgetag CC, van Ooyen A. 2009. A simple rule for axon outgrowth and synaptic competition generates realistic connection lengths and filling fractions. *Cereb Cortex*. 19(12):3001–3010.

Karbowski J. 2001. Optimal wiring principle and plateaus in the degree of separation for cortical neurons. *Phys Rev Lett*. 86(16):3674–3677.

Kolmogorov A. 1933. Sulla determinazione empirica di una legge di distribuzione. *G Ist Ital Attuari*. 4:83–91.

Kötter R. 2004. Online retrieval, processing, and visualization of primate connectivity data from the CoCoMac database. *Neuroinformatics*. 2(2):127–144.

Laughlin SB, Sejnowski TJ. 2003. Communication in neuronal networks. *Science*. 301(5641):1870–1874.

Lewis JW and Van Essen DC. 2000. Mapping of architectonic subdivisions in the macaque monkey, with emphasis on parieto-occipital cortex. *J Comp Neurol* 428(1):79–111.

Linsker R. 1988. Self-organization in a perceptual network. *Computertomographie*. 21(3):105–117.

Goldman-Rakic PS, Rakic P. 1991. Preface: cerebral cortex has come of age. *Cereb Cortex*. 1(1):1.

Meunier D, Lambiotte R, Bullmore ET. 2010. Modular and hierarchically modular organization of brain networks. *Front Neurosci*. 4:200.

Muller L, Chavane F, Reynolds J, Sejnowski TJ. 2018. Cortical travelling waves: mechanisms and computational principles. *Nat Rev Neurosci*. 19(5):255.

Newman MEJ. 2006. Modularity and community structure in networks. *Proc Natl Acad Sci U S A*. 103(23):8577–8582.

Oh SW, Harris JA, Ng L, Winslow B, Cain N, Mihalas S, Wang Q, Lau C, Kuan L, Henry AM, et al. 2014. A mesoscale connectome of the mouse brain. *Nature*. 508(7495):207–214.

Picco N, García-Moreno F, Maini PK, Woolley TE, Molnár Z. 2018. Mathematical modeling of cortical neurogenesis reveals that the founder population does not necessarily scale with neurogenic output. *Cereb Cortex*. 28(7):2540–2550.

Ramon-y-Cajal S, et al. 1996. Histology of the nervous system. *Trends Neurosci*. 19(4):156.

Roberts JA, Gollo LL, Abeysuriya RG, Roberts G, Mitchell PB, Woolrich MW, Breakspear M. 2019. Metastable brain waves. *Nat Commun*. 10(1):1056.

Rubino D, Robbins KA, Hatsopoulos NG. 2006. Propagating waves mediate information transfer in the motor cortex. *Nat Neurosci*. 9(12):1549.

Rubinov M, Sporns O. 2011. Weight-conserving characterization of complex functional brain networks. *Neuroimage*. 56(4):2068–2079.

Rubinov M, Ypma RJF, Watson C, Bullmore ET. 2015. Wiring cost and topological participation of the mouse brain connectome. *Proc Natl Acad Sci U S A*. 112(32):10032–10037.

Shannon CE. 1948. A mathematical theory of communication. *Bell Syst Tech*. 27(3):379–423.

Smirnov N. 1948. Table for estimating the goodness of fit of empirical distributions. *Ann Math Stat*. 19(2):279–281.

Song HF, Kennedy H, Wang X-J. 2014. Spatial embedding of structural similarity in the cerebral cortex. *Proc Natl Acad Sci U S A*. 111(46):16580–16585.

Sporns O, Betzel RF. 2016. Modular brain networks. *Annu Rev Psychol*. 67:613–640.

Stepanyants A, et al. 2007. Local potential connectivity in cat primary visual cortex. *Cereb Cortex*. 18(1):13–28.

Stiso J, Bassett DS. 2018. Spatial embedding imposes constraints on neuronal network architectures. *Trends Cogn Sci*. 22(12):1127–1142.

Toker D, Sommer FT. 2019. Information integration in large brain networks. *PLoS Comp Biol*. 15(2):e1006807.

van den Heuvel MP, Kahn RS, Goni J, Sporns O. 2012. High-cost, high-capacity backbone for global brain communication. *Proc Natl Acad Sci U S A*. 109(28):11372–11377.

Varshney LR, et al. 2011. Structural properties of the Caenorhabditis elegans neuronal network. *PLoS Comp Biol*. 7(2):1–21.

Watts DJ, Strogatz SH. 1998. Collective dynamics of "small-world" networks. *Nature*. 393(6684):440–442.

White JG, Southgate E, Thomson JN, Brenner S. 1986. The structure of the nervous system of the nematode Caenorhabditis elegans. *Philos Trans R Soc Lond B Biol Sci*. 314(1165):1–340.

Young MP. 1992. Objective analysis of the topological organization of the primate cortical visual system. *Nature*. 358(6382): 152–155.

Zhou D, Xiao Y, Zhang Y, Xu Z, Cai D. 2013. Causal and structural connectivity of pulse-coupled nonlinear networks. *Phys Rev Lett*. 111(5):054102.

Supplementary Material for

Maximum entropy principle underlies wiring length distribution in brain networks

Yuru Song, Douglas Zhou, Songting Li

D.Z. zdz@sjtu.edu.cn
S.L. songting@sjtu.edu.cn

This PDF file includes:

Supporting Information Text

Analysis of the structure-function relation of an idealized brain network. It is generally believed that the structure of a brain network supports its functional efficiency. Previous works suggest that one of the functional efficiency of brain information processing can be evaluated by the average shortest path (ASP) of the network[1] reflecting the communication speed or the time it takes a neuronal signal to transmit from one area to another area on average.[2] In the main text, we have shown that the brain network possesses the feature of structural diversity. Here we reveal the relation between structural diversity and functional efficiency using theoretical analysis of an idealized brain network, which indicates that large structural diversity leads to small ASP that supports and benefits information transmission in brain networks.

We first build an idealized brain network based on Ref.,[3] in which ASP has been analytically calculated. As shown in Supporting Material Fig 6A, in the idealized network, we consider L brain areas located evenly in a ring lattice. Each area connects to its nearest $2k$ neighboring areas. In addition, a certain number of long-range shortcuts are added to the network to connect pairs of areas chosen randomly. The number of shortcuts are determined by the probability ϕ per connection on the underlying ring lattice such that the total number of shortcuts is $Lk\phi$ on average. By introducing a characteristic length parameter $\xi = 1/(k\phi)$, the average number of shortcuts becomes L/ξ, and the value of ASP can be calculated as[3]

$$\mathrm{ASP} = \frac{\xi}{2k\sqrt{1+2\xi/L}} \tanh^{-1} \frac{1}{\sqrt{1+2\xi/L}}.$$

To calculate the wiring entropy of the network, we first describe the spatial location of each area in the ring network by an angular coordinate $2\pi i/L, (i = 1, 2, \ldots, L)$. Subsequently, the distance between the i-th and j-th areas can be calculated as $2\pi|i-j|/L$ in the angular space. To simplify the calculation, we assume L is an even number, thus the smallest and largest wiring lengths are $2\pi/L$ and π respectively. We then discretize the wiring length distribution by dividing the distance range into $L/2$ bins evenly, which are $[\frac{3\pi}{2L}, \frac{5\pi}{2L}), [\frac{5\pi}{2L}, \frac{7\pi}{2L}), \ldots, [\pi - \frac{\pi}{2L}, \pi + \frac{\pi}{2L})$. If the probability ϕ for adding a shortcut is zero, there are only L links belonging to each of the first k bins and there is no link in the remaining bins. Whereas if ϕ is nonzero, an average number of $Lk\phi$ shortcuts will be randomly and independently added to the network, hence the lengths of those shortcuts will fall into all the $L/2$ bins with equal probability. Therefore, the number of shortcuts in each of the the $L/2$ bins is $2k\phi$ on average. Accordingly, the connection length distribution is approximately

$$P(d \in i\text{th bin}) = \begin{cases} \frac{L}{kL+(L/2-k)2k\phi} & \text{for } i \le k \\ \frac{2k\phi}{kL+(L/2-k)2k\phi} & \text{for } i > k \end{cases}$$

based on which we can calculate the wiring entropy as

$$H = -\frac{kL\xi}{kL\xi+L-2k}\ln(L\xi) - \frac{L-2k}{kL\xi+L-2k}\ln(2) + \ln(kL\xi+L-2k).$$

As shown in Supporting Material Fig 6B, as the parameter ϕ increases, the wiring entropy increases while the ASP decreases. Therefore, larger wiring entropy in this idealized brain network corresponds to smaller ASP of the network, which supports fast communications between brain areas. Note that by increasing ϕ, the idealized network gradually evolves from regular-lattice network towards small-world network. The latter possesses the features of high clustering coefficient and short ASP, which are similar to those observed in certain real brain networks. Therefore, the functional implication of large entropy for supporting efficient communications in the idealized network may also be valid in some brain networks.

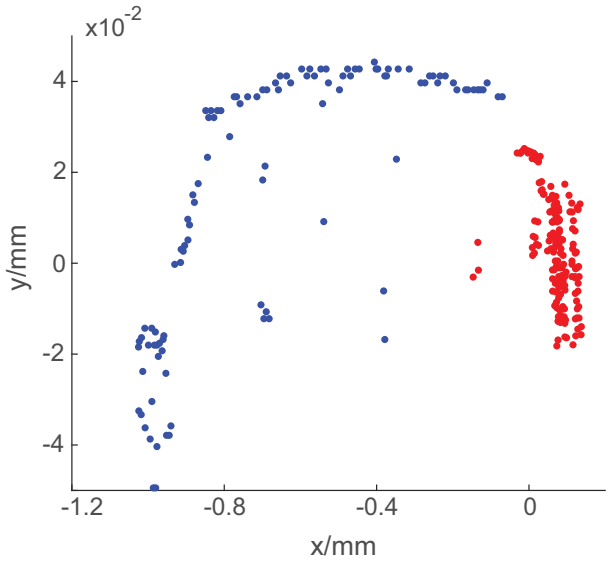

Fig 1. The spatial layout of neurons in *C. elegans*. Each dot represents a neuron. Neurons marked by red compose the local network of *C. elegans*. The coordinates represent the locations of each neuron in the actual body in the unit of mm.

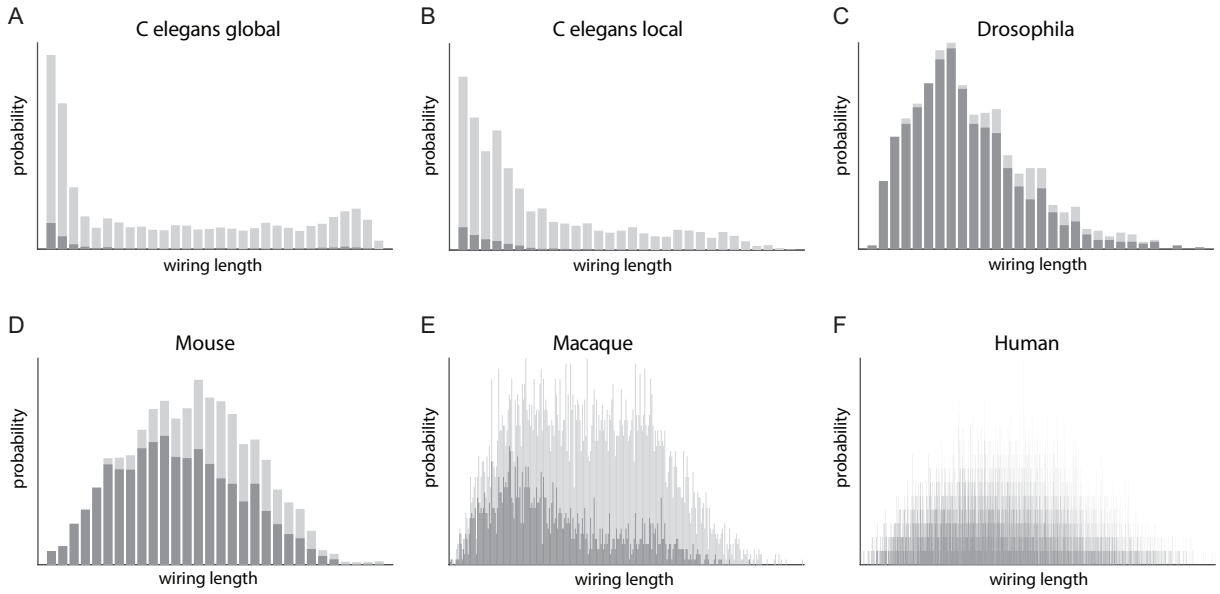

Fig 2. Wiring length distributions of brain networks across multiple species using the same bin size. (A)-(F) are for the global and local neural networks of C. elagans, and the brain networks of Drosophila, mouse, macaque, human, respectively. In each panel, dark gray bars are the wiring length distribution measured from experiments. Light gray bars are the upper bound of the wiring length distribution given by the reference distribution defined in the main text. (A)-(C) use the same bin size of 9.5 μm, and (D)-(F) use the same bin size of 382 μm.

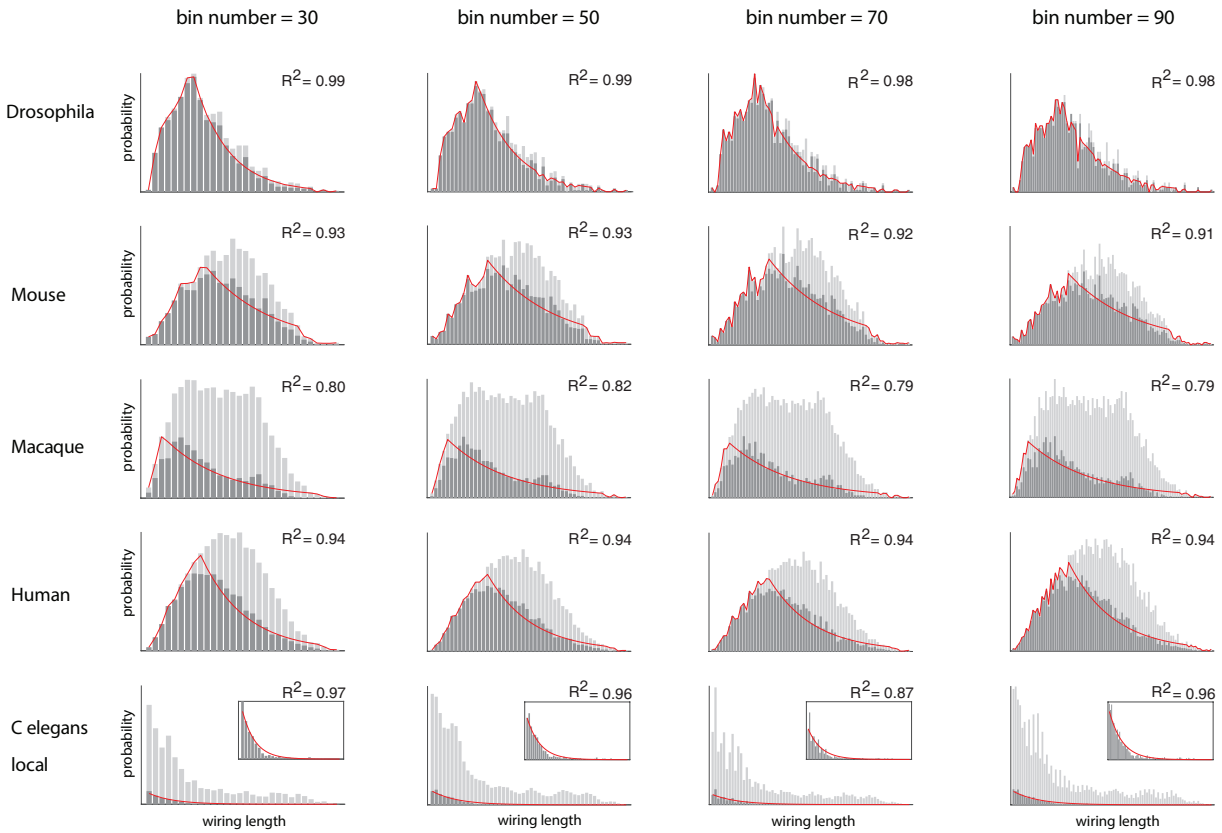

Fig 3. Wiring length distributions of brain networks across multiple species and their predictions by the maximum entropy principle using different bin numbers. Each row corresponds to one species, and each column corresponds to the choice of a particular bin number. In each panel, dark gray bars are the wiring length distribution measured from experiments. Light gray bars are the upper bound of the wiring length distribution given by the reference distribution defined in the main text. Red solid line is the wiring length distribution predicted by the maximum entropy principle (Eqs. 1- 4 in the main text). R2 is calculated to evaluate the performance of the prediction.

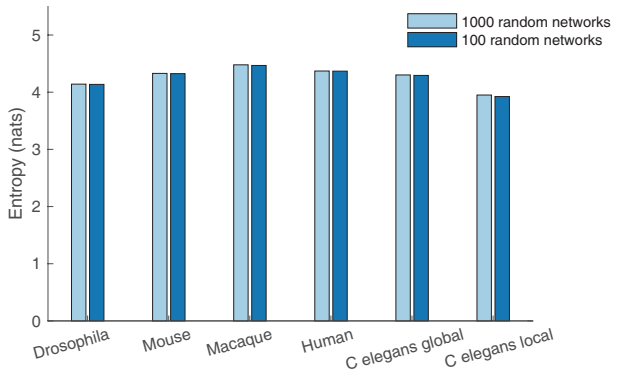

Fig 4. Comparison between the largest wiring entropy from 100 random networks with that from 1000 random networks. The small difference indicates that the largest wiring entropy value of 100 random networks well approximates the upper bound of each brain network's wiring entropy.

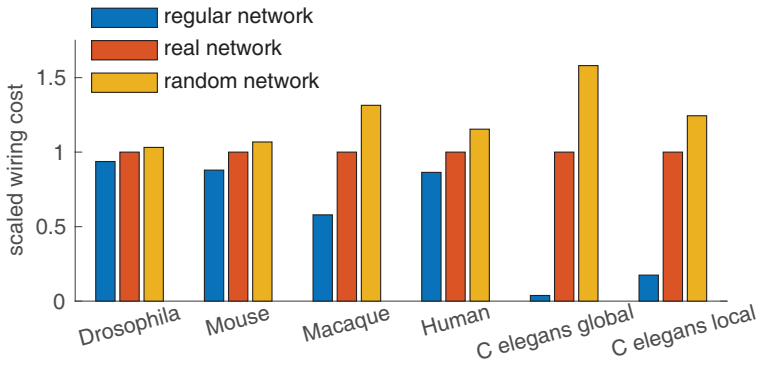

Fig 5. Scaled wiring cost of the six brain networks. All the network material costs are normalized by the real network material cost. Red bars correspond to the wiring cost of Drosophila, mouse, macaque, human, the global and local networks of C. elegans. Blue and yellow bars are the wiring costs of the corresponding regular network and random network, respectively.

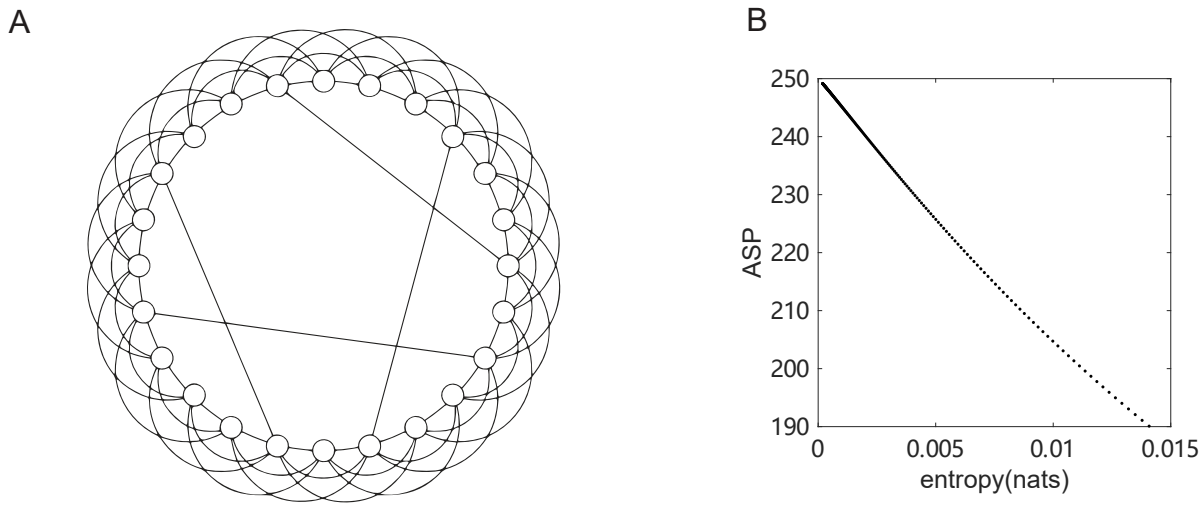

Fig 6. Negative correlation between wiring entropy and ASP revealed in an idealized brain network. (A) A schematic graph of an idealized brain network with 24 areas and 4 shortcuts. Each area connects to its nearest 6 neighboring areas. (B) ASP negatively correlates with wiring entropy derived from the mathematical analysis. The network has 1000 areas and each area connects to its nearest 2 neighbors.

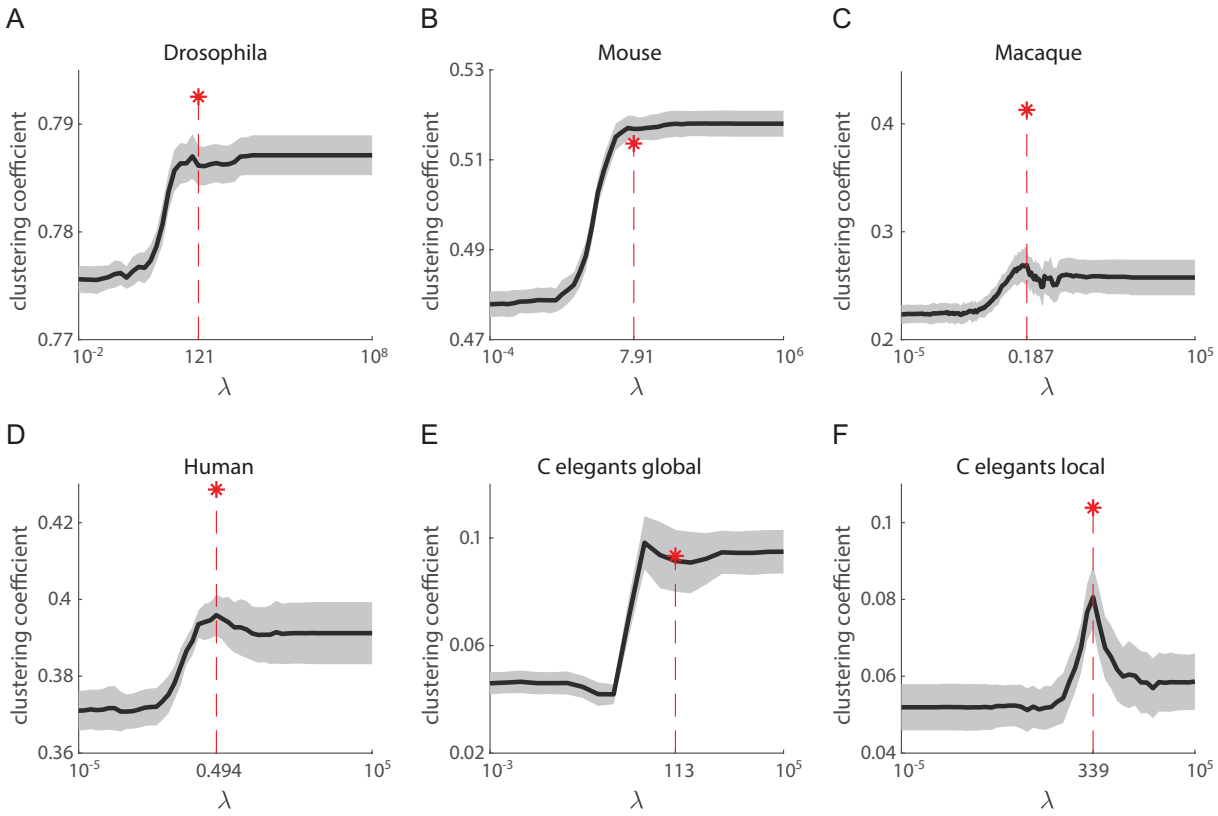

Fig 7. The dependence of clustering coefficient on λ in the ECD model. (A) *Drosophila* network. (B) Mouse network. (C) Macaque network. (D) Human network. (E) Global network of *C. elegans*. (F) Local network of *C. elegans*. The black line is the average clustering coefficient. The shaded grey area as the standard deviation calculated from multiple trials of realization. The red star shows the clustering coefficient value of the corresponding real brain network. The vertical red dashed line together with its value on the abscissa indicates the λ value for the best performance ECD generative network. λ is in the unit of mm^{-1}.

Table 1. Parameters in the random growth model for the six brain networks.

	Number of outgrowing axons	Radius of touching area in unit of network size	Growth speed	Failure probability of synapse formation
Drosophila	200	0.43	0.1	0.5
Mouse	200	0.2	0.1	0.5
Macaque	200	0.13	0.1	0.5
Human	200	0.173	0.1	0.5
C. elegans global	50	0.2	0.2	0.8
C. elegans local	40	0.2	0.2	0.965

Table 2. Maximum entropy principle applied to a variety of transport networks.

Network	R-square	Data source
US Airport	0.92	[4]
Shanghai Metro	1	[5]
Venice Bus	1	[6]
Sydney Rail	0.92	[6]
Sydney Ferry	0.99	[6]
Sydney Bus	1	[6]
Paris Trolley	1	[6]
Paris Subway	0.99	[6]
Paris Rail	0.99	[6]
Paris Bus	1	[6]
Melbourne Trolley	1	[6]
Melbourne Rail	0.95	[6]
Melbourne Bus	1	[6]
Lisbon Subway	0.95	[6]
Lisbon Rail	0.94	[6]
Berlin Trolley	1	[6]
Berlin Subway	1	[6]
Berlin Rail	0.96	[6]

References

1. Watts DJ, Strogatz SH (1998) Collective dynamics of 'small-world'networks. *nature* 393(6684):440.
2. Bullmore E, Sporns O (2012) The economy of brain network organization. *Nature Reviews Neuroscience* 13(5):336.
3. Newman ME, Moore C, Watts DJ (2000) Mean-field solution of the small-world network model. *Physical Review Letters* 84(14):3201.
4. https://openflights.org/data.html.
5. http://service.shmetro.com/czxx/index.htm.
6. Kujala R, Weckstrom C, Darst RK, Mladenovic MN, Saramaki J (2018) A collection of public transport network data sets for 25 cities. *Scientific Data* 180089.